Food Science of Animal Resources

Food Sci. Anim. Resour. 2020 September 40(5):813~830
DOI https://doi.org/10.5851/kosfa.2020.e60

pISSN : 2636-0772 eISSN : 2636-0780
http://www.kosfaj.org

ARTICLE

Infrared Assisted Freeze-Drying (IRAFD) to Produce Shelf-Stable Insect Food from *Protaetia brevitarsis* (White-Spotted Flower Chafer) Larva

Apinya Khampakool[1], Salinee Soisungwan[1], SangGuan You[1], and Sung Hee Park[2,*]

[1]Department of Marine Food Science and Technology, Gangneung-Wonju National University, Gangneung 25457, Korea
[2]Department of Food Science and Technology, Seoul National University of Science and Technology, Seoul 01811, Korea

OPEN ACCESS

Received July 13, 2020
Revised July 28, 2020
Accepted July 28, 2020

***Corresponding author** : Sung Hee Park
Department of Food Science and Technology, Seoul National University of Science and Technology, Seoul 01811, Korea
Tel: +82-2-970-6621
Fax: +82-2-976-6460
E-mail: sunghpark@seoultech.ac.kr

***ORCID**
Apinya Khampakool
https://orcid.org/0000-0001-5843-3325
Salinee Soisungwan
https://orcid.org/0000-0002-0803-6572
SangGuan You
https://orcid.org/0000-0002-8785-7167
Sung Hee Park
https://orcid.org/0000-0002-2755-2863

Abstract In this study, the potential of infrared assisted freeze-drying (IRAFD) was tested for the production of shelf-stable edible insects: *Protaetia brevitarsis* larva (larva of white-spotted flower chafer). The IRAFD system was customized using an infrared lamp, K-type thermocouple, controller, and data acquisition system. The infrared lamp provided the sublimation energy for rapid freeze-drying (FD). The IRAFD conditions were continuous IRAFD-5.0 kW/m^2 and IRAFD-5.0 kW/m^2 at different weight reduction (WR) (10%, 20%, and 30%). The continuous IRAFD reduced the drying time to 247 min compared to the 2,833 min duration of FD ($p<0.05$). The electrical energy could be reduced by more than 90% through infrared radiation during FD ($p<0.05$). The Page model resulted in the best prediction among the tested drying kinetic models. In terms of quality, IRAFD showed significantly lower hardness, chewiness, and higher protein levels than hot air drying and FD ($p<0.05$). IRAFD better preserved the glutamic acid (6.30–7.29 g/100 g) and proline (3.84–5.54 g/100 g). The external product appearance after IRAFD exhibited more air pockets and volume expansion, which might result in a good consumer appeal. In conclusion, this study reports the potential of IRAFD in producing shelf-stable and value-added edible insects.

Keywords infrared assisted freeze-drying, insect, energy, efficiency, texture

Introduction

Insects have been used as valuable food sources for human consumption for a long time in Africa, Asia, and Latin America (Alves et al., 2016). Several edible insects have been studied for their potential of insect protein contents, such as mealworm larva (*Tenebrio molitor*), silkworm pupae (*Bombyx mori*), and white-spotted flower chafer larva (*Protaetia brevitarsis*) (Chung et al., 2013; Melis et al., 2018). *P. brevitarsis* larva is one of the most popular insects in East Asia, including Korea, Japan, Taiwan, and China. In particular, *P. brevitarsis* larvae have shown beneficial pharmaceutical

effects in cancer, inflammation, liver cirrhosis, and hepatitis (Jeong et al., 2020; Lee et al., 2017).

Once a cold chain system is not available, freeze-drying (FD) is often applied for insect preservation (Baiano, 2020; Klunder et al., 2012). FD is a commercially used for stabilization of insects as food in the industry (Kröncke et al., 2018). It provides good quality attributes with low processing temperatures (Kröncke et al., 2018). Although good product quality of FD is advantage, it has limitations as slow processing with the ice sublimation taking a longer time than vaporization (Khampakool et al., 2019). Hybrid FD technologies have been investigated with combination of other drying methods (microwave, infrared, ultrasonic) for rapid FD (Chakraborty et al., 2011; Khampakool et al., 2019). Recently, the combination of IR and FD showed the efficiency of rapid drying and good quality retention of agricultural product drying (Baeghbali et al., 2020; Khampakool et al., 2019). The IR radiative energy penetrates into surface layer of wet porous product, creating molecular vibration and providing thermal energy for an enhanced drying rate during FD (Khampakool et al., 2019; Lin et al., 2005). Although there have been several previous studies on infrared assisted freeze-drying (IRAFD) for agricultural products, in our best knowledge, none of them described drying insects as food using the IRAFD technique. Therefore, the potential of IRAFD was investigated for the rapid FD of insects (*P. brevitarsis*) as foods associated with drying kinetics, energy efficiency, textural qualities, and nutritional aspects.

Materials and Methods

Insect samples and blanching

Living *P. brevitarsis* larvae were obtained from a local farm (Gangneung, Korea). Larva samples were fasted for 24 h in order to clear any gastrointestinal feces as suggested by Zielińska et al. (2015), then washed to remove any residuals. Blanching in boiling water is essential to eliminate most of the present insect Enterobacteriaceae (Klunder et al., 2012). In this study, 400 g of larvae was blanched in 4 L of boiling water for 40 s, then chilled in refrigerated water for 60 s. This procedure was suggested by Vandeweyer et al. (2017). The blanched sample was sieved to eliminate the residual water, and one batch sample (total 40 g) was placed into a Petri dish covered with parafilm. They were frozen in an air blast freezer at –50°C until further use.

IRAFD experimental setup

Fig. 1 presents a schematic diagram of the semi-customized IRAFD system used in a previous study (Khampakool et al., 2019, Elsevier and Copyright Clearance Center License Number 4866430761862). The IRAFD unit was equipped with a cylindrical acrylic chamber (diameter: 290, height: 400 mm), oil rotary vacuum pump (JBA00089, Jungwoo Motor, Hanam, Korea), a refrigeration system down to –100°C, and a 250 Watt-powered near-infrared lamp (BR 125, Koninklijke Philips N.V., Andover, MA, USA). A digital balance (CB-300, A&D, Seoul, Korea) and an RS 232 cable were connected in the vacuum chamber. This enabled to record the weight changes in the sample during the IRAFD experiment. The infrared intensity was controlled using a variable alternating current transformer (Model 3-5-44, Paju, Korea) at 60 Hz. The temperature, voltage, and current in the IRAFD system were monitored and collected every 3 s using a data acquisition system (DAQ, 34972A, Keysight, Santa Clara, CA, USA). These data were used to evaluate the energy efficiency of the IRAFD system. The energy consumptions of the pump and condenser were analyzed using an electric energy meter (SJPM-16, SEOJUN Electric., Seoul, Korea), as described in our previous work (Khampakool et al., 2019).

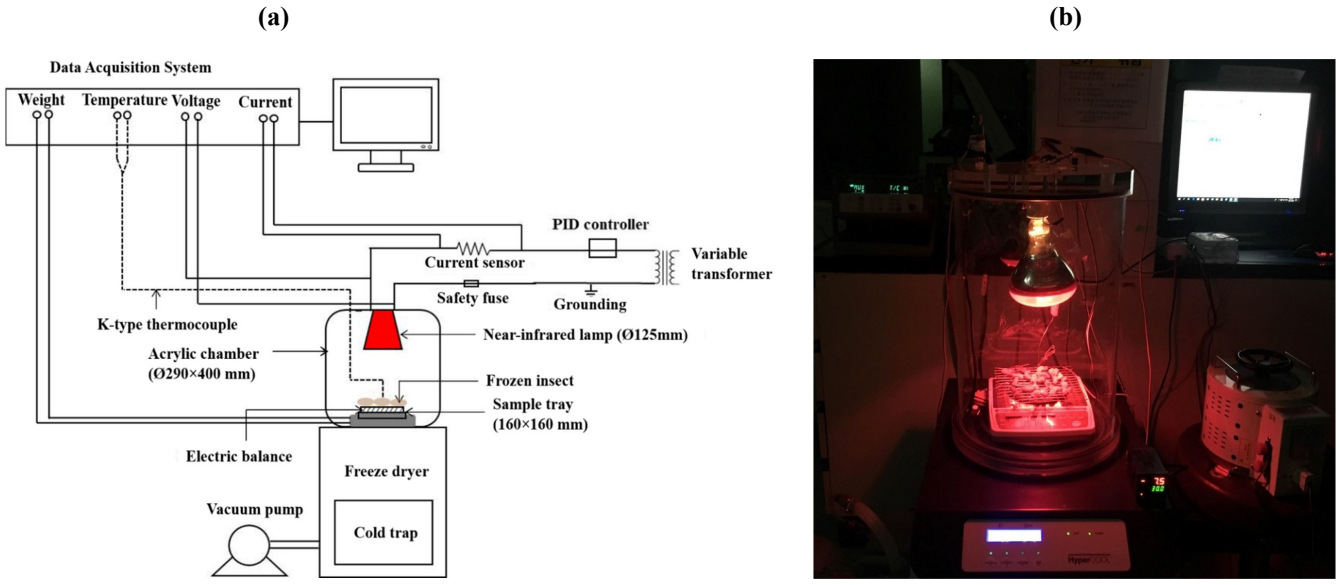

Fig. 1. Infrared assisted freeze drying (IRAFD) system: (a) schematic diagram and (b) photo image (reproduced and modified with permission from Khampakool et al., 2019: Elsevier and Copyright Clearance Center License Number 4851920028217). IRAFD, infrared assisted freeze-drying.

IRAFD trials

The frozen larva sample (25 disks, total 40 g) was placed on the tray of #4 mesh (4.76 × 4.76 mm) above the balancing system. A distance of 150 mm was maintained between the sample and an IR lamp. In this study, four different IRAFD conditions were tested with a combined effect of IR power intensity and IR radiation initiation stage as follows: 1) FD without IR, 2) Continuous IRAFD-5.0 kW/m^2, 3) IRAFD-5.0 kW/m^2 at 10% WR, 4) IRAFD-5.0 kW/m^2 at 20% WR, and 5) IRAFD-5.0 kW/m^2 at 30% WR. IRAFD process parameters were optimized in a previous study (Khampakool et al., 2019) and preliminary experiments (data not shown) which does not induce the collapse phenomenon of samples.

In the case of the FD, the samples were freeze-dried without IR radiation under a vacuum of 6.67 Pa and cold trap temperature at –100°C. In case of the continuous IRAFD, a variable power (AC) supplier provided IR radiant energy of 5.0 kW/m^2 from the initial stage to the final stage during FD at 6.67 Pa. In the IRAFD-5.0 kW/m^2 at 10% WR, the IR lamp was turned off at the initial stage of FD, then the IR lamp was turned on at 5.0 kW/m^2 power after the sample weight was reduced by 10% to its initial weight. For the IRAFD-5.0 kW/m^2 at 20% WR and the IRAFD-5.0 kW/m^2 at 30% WR, the IR lamp was shut down at 5.0 kW/m^2 power when the weight of sample was reduced by 20% and 30% to their initial weight, respectively. Each condition was replicated three times. Larva samples were dried until the final moisture content (moisture ratio, MR) reached <0.20.

Hot air drying of insects was conducted at 70°C for 4 h to compare their external appearance, protein content, content of essential amino acids, and content of non-essential amino acids using a hot air dryer (OF-02GW, PNC Trading, Seoul, Korea) at 70°C for 4 h.

Radiant energy

Radiant energy from IR lamp provided the drying force of ice sublimation; thus, the total energy used to sublime ice was estimated as shown in Eq. (1) as suggested (Khampakool et al., 2019).

$$E_{tl} = E_{vc} + E_{rd} \quad (1)$$

where E_{tl} is the total energy (J), E_{vc} is the vacuum energy (J), and E_{rd} is the radiant energy (J).

The total energy for ice sublimation from the initial (M_0) to the final moisture content (M_f), as shown in Eq. (2), as suggested by Khampakool et al. (2019).

$$E_{tl} = W \times (M_0 - M_f) \times L_s \quad (2)$$

where E_{tl} is the total energy (J), W is the weight of the sample (kg), M_0 is the initial mass fraction of moisture (0.70), M_f is the final mass fraction of moisture (0.20), L_s is the latent heat for ice sublimation (L_S, 2.834×10^3 kJ·kg^{-1}) (Khampakool et al., 2019; Zdunkowski and Bott, 2004). Subsequently, E_{tl} the value was calculated as 991,900 J.

The vacuum energy (E_{vc}) of FD is 991,900 J, which is the same as E_{tl} that of IRAFD, as only vacuum worked as the driving force of ice sublimation under vacuum during FD as previous study reported (Khampakool et al., 2019). All the IRAFD trials decreased the total drying time when compared to that of FD, which meant that the samples were stayed for a shorter time at vacuum condition and reduced vacuum energy, as presented in a previous work (Khampakool et al., 2019). Subsequently, the vacuum energy of each IRAFD trial ($E_{vc,IRAFD}$) was calculated as the ratio of IRAFD drying time (t_{IRAFD}) to FD drying time (t_{FD}), as suggested by previous study (Khampakool et al., 2019) in Eq. (3).

$$E_{vc,IRAFD} = E_{tl} \times \frac{t_{IRAFD}}{t_{FD}} \quad (3)$$

Although reduced vacuum energy (E_{vc}) was applied to IRAFD samples, radiant energy (E_{rd}) supplied a greater driving force for the ice sublimation. The radiant energy (E_{rd}) was estimated as shown in Eq. (4) (Khampakool et al., 2019).

$$E_{rd,IRAFD} = E_{tl} - E_{vc,IRAFD} \quad (4)$$

where $E_{rd,IRAFD}$ is the radiant energy of IRAFD (J), and $E_{vc,IRAFD}$ is the vacuum energy of IRAFD (J).

Drying kinetic models

The moisture content of the drying sample at time t was expressed as the MR, as shown in Eq. (5). MR provides a good understanding of the drying kinetics during the drying experiment.

$$MR = \frac{M - M_e}{M_0 - M_e} \quad (5)$$

where M is the dry basis moisture content at an arbitrary time, M_e is the equilibrium final moisture content, and M_o is the initial dry basis moisture content.

In this study, the obtained MR data were fitted into three mathematical models (Exponential model, Page model, Simplified diffusion model) to select the appropriate model to explains the behavior of drying kinetics for each drying experiment. In

this study, a non-linear slope was observed for all the drying experiments. Thus, most commonly used non-linear drying kinetics were adopted.

Exponential model

The most simplified nonlinear drying model is known as the exponential model, as shown in Eq. (6) (Simal et al., 2005).

$$MR = \exp(-k \cdot t) \tag{6}$$

where MR is the moisture ratio, k is the drying constant (min^{-1}), and t is time (min).

Exponential assumes that internal resistance could be neglected with no resistance to moisture transfer from central position to the surface (Kashaninejad et al., 2007).

Page model

The Page model adopts two constant empirical modifications of the exponential model, where it produces good fits to describe the drying of various foods and agricultural products (Doymaz, 2011; Kashaninejad et al., 2007; Page, 1949). The Page model is presented as shown in Eq. (7).

$$MR = \exp(-k \cdot t^N) \tag{7}$$

where MR is the moisture ratio, k is the drying constant, t is time (min), and N is the shape factor.

Simplified diffusion model

Fick's second law of diffusion has been developed to describe the falling rate drying period for most food and agricultural products as a simplified diffusion model (Khampakool et al., 2019; Sacilik, 2007) as shown in Eq. (8).

$$MR = \frac{M}{M_0} = \frac{8}{\pi^2} \times \exp\left[-\pi^2 \frac{D_{eff} t}{4L^2}\right] \tag{8}$$

where MR is the moisture ratio, M is the moisture content at an arbitrary time, M_0 is the initial moisture content, D_{eff} is the diffusion coefficient (m^2/min), L is the half-thickness of the sample (mm), and t is time (min).

Electrical energy consumption

Energy consumption should be critically considered in the drying process (Khampakool et al., 2019). Thermal drying operations consumes 10%–25% of the national industrial energy in almost all industrial sectors according to various calculations (Hafezi et al., 2014). In this study, the electrical equipment (vacuum pump, condenser, and IR lamp) of the IRAFD system were considered to evaluate the total energy consumption. The electrical energy meter (SJPM-16, SEOJUN Electronics, Seoul, Korea) measured the electricity consumption (J) of the vacuum pump and condenser. The energy consumption of the IR lamp was estimated with voltage and current data through Ohm's law and its integration versus time as

shown in Eq. (9) as suggested by previous work (Khampakool et al., 2019).

$$E_{ir} = \int_{t_i}^{t_f} I \cdot V dt \quad (9)$$

where E_{ir} is the energy consumption of IR lamp (kJ), I is current (A), V is voltage (V), and t is drying time (s). Eq. 9 was solved using trapezoidal numerical integration of MATLAB software (Version 2019b, Mathworks INC, MA, USA) as suggested by previous studies (Park and Jo, 2019; Park et al., 2014).

Texture profile analysis

The texture of dried larva samples was measured using a TA-XT Plus Texture Analyzer (Texture Technology, Brewster, NY, USA). Hardness (N) and chewiness of dried insects were estimated. Dried insect samples obtained from each condition were placed on an acrylic tubing (Ø18 mm) and tested using a P.2-cylinder probe. The texture analyzer was set for the following test conditions: pre-test speed at 1.0 mm/s, test speed at 1.0 mm/s, post-test speed at 5.0 mm/s, target distance at 5.0 mm, time at 5.0 sec, and trigger type Auto. Hardness and chewiness were estimated. Hardness values were acquired from the peak force of the force-deformation curve. The chewiness was calculated as the product of hardness×springiness× cohesiveness value.

Changes in external size

IRAFD treated samples showed volume expansion; thus, changes in external size were analyzed using photo images. Images of dried larva samples were taken after the FD and IRAFD trials, and external size was measured using image analysis program (ImageJ software version 1.52 h, National Institute of Health, Bethesda, MD, USA). The photo image of sample was taken from top position and then cross sectional area was drawn using image analysis program. Image analysis was conducted at vertical direction of sample; so, it provided the cross sectional area of dried larva. In this study, this cross sectional area was considered as external size (mm^2). The external size (mm^2) indicates the size expansion of dried larva samples during different drying methods. Initial size of sample before drying was 270±8 mm^2.

Protein and amino acid analyses

The protein content was determined by the Kjeldahl method (Chang, 2010) as described below. Kjehdal analysis of protein followed the method 918.10 of the AOAC international (AOAC, 2016). The analysis Crude protein was estimated as the average nitrogen content (N)×6.25. Amino acid groups were determined following the method of Chung et al. (2013). A sample of 5 g was dissolved in 40 mL of 6 N HCl into a round bottom flask. The dissolved sample mixture was hydrolyzed by N_2 injection at 110℃ for 24 h. The hydrochloric acid was concentrated under vacuum at 50℃. The concentrated solution was diluted with 50 mL of 0.2 N sodium citrate buffer (pH=2.2) and filtered with filter paper (0.45 μm). The filtered sample (30 μL) was analyzed using an amino acid analyzer (L-8900, Hitachi, Minato, Tokyo, Japan).

Statistical analysis

Fisher's least-significant difference (LSD) analysis were selected for multiple comparisons among experiments at the 95%

confidence interval ($p<0.05$). The data were analyzed using Statistical Analysis System (SAS) software (version 9.1.3, SAS Inst., Cary, NC, USA). Statistical analysis was performed using analysis of variance (ANOVA) for multiple comparisons. All experiments were repeated in triplicate.

Results and Discussion

Drying curves and temperature profiles during the FD and IRAFD trials

Drying curves and temperature evolution of FD and different IRAFD trials are compared for *P. brevitarsis* larva in Fig. 2. The longest drying time and drying rate were found at FD of 2,833±88 min and 0.65±0.04 g/h, respectively, with the vacuum energy of 992±0 kJ which is driving force of ice sublimation (Table 1). The initial temperature of the FD dried larvae was –27.2±5°C and the final temperature was 15.7±3°C. The FD process usually proceeds in three steps: freezing, the primary drying step, and the secondary drying step (Ciurzyńska and Lenart, 2011). In the primary step of FD, the sublimation rate gradually decreases due to the internal heat and mass rate decrease during the thickness of the dried layer develops (Jin et al., 2018). Hence, the secondary drying state usually takes approximately 1/3 or 1/2 time of primary drying (Nireesha et al., 2013).

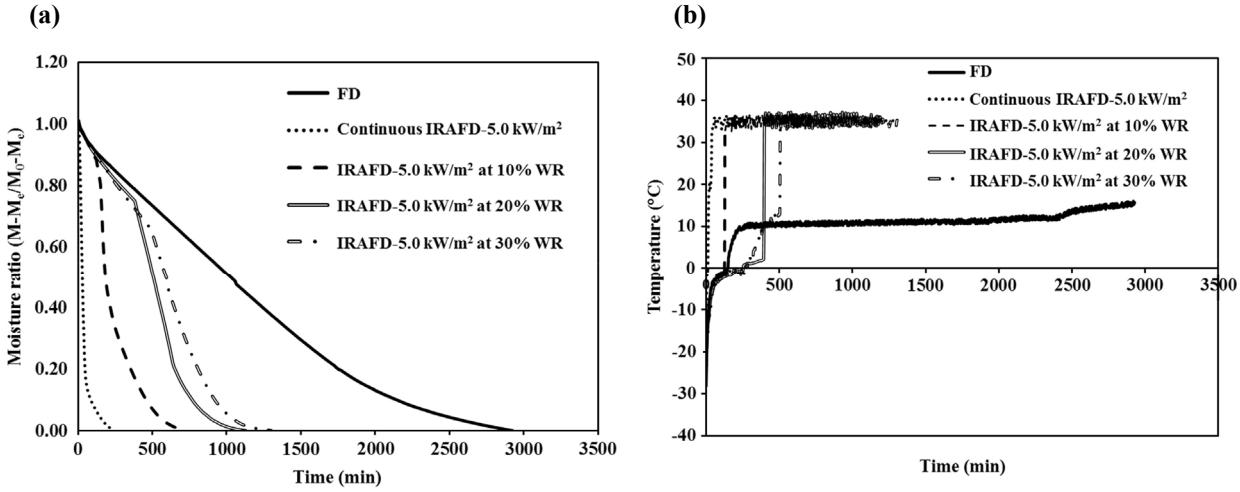

Fig. 2. (a) Moisture ratio and (b) temperature profiles of *Protaetia brevitarsis* larva during FD and different IRAFD trials. FD, freeze-drying; IRAFD, infrared assisted freeze-drying; WR, weight reduction.

Table 1. Drying time, drying rate, vacuum energy (kJ), and radiant energy (E_{rd}, kJ) of FD and different IRAFD trials for dried *P. brevitarsis* larva

Methods	Total drying time (min)	10% WR (min)	20% WR (min)	30% WR (min)	Drying rate (g/h)	Vacuum energy (kJ)	Radiant energy (E_{rd}, kJ)
FD	2,833±88^{a}	188±9^{a}	475±5^{a}	758±7^{a}	0.65±0.04^{d}	992±0^{a}	-
Continuous IRAFD-5.0 kW/m^2	247±9^{e}	16±2^{e}	22±3^{d}	25±2^{e}	7.17±0.15^{a}	87±5^{e}	905±5^{a}
IRAFD-5.0 kW/m^2 at 10% WR	736±30^{d}	125±4^{d}	156±3^{c}	171±4^{d}	2.57±0.25^{b}	258±11^{d}	734±11^{b}
IRAFD-5.0 kW/m^2 at 20% WR	1,168±33^{c}	160±8^{c}	390±3^{b}	444±16^{c}	1.55±0.04^{c}	409±24^{c}	583±24^{c}
IRAFD-5.0 kW/m^2 at 30% WR	1,331±52^{b}	173±5^{b}	381±10^{b}	503±8^{b}	1.42±0.07^{c}	477±31^{b}	515±31^{d}

$^{a–e}$ Means (±SD) with a different letter in the same column are significantly different at $p<0.05$.
FD, freeze-drying; IRAFD, infrared assisted freeze-drying; WR, weight reduction.

These authors proposed that this leads to long drying time of FD and increases processing cost.

Continuous IRAFD-5.0 kW/m^2 had the shortest drying time of 247±9 min with a drying rate of 7.17±0.15 g/h. The drying time was reduced by 90% compared with FD ($p<0.05$) with the highest radiant energy (E_r) of 905±5 kJ (Table 1). The product temperature elevated from –27.6℃ to 34.8℃. IR radiation might save the secondary drying time since energy of IR should work as a driving force for desorption (Khampakool et al., 2019). The gradient of MR showed a drastic decline within 48 min. Infrared radiation penetrates food materials and then accelerates heating and enhances the drying rate (Wang et al., 2019).

The IRAFD-5.0 kW/m^2 at 10% WR took the total drying time of 736±30 min and drying rate of 2.57±0.25 g/h. The drying time was reduced by 74% compared with FD ($p<0.05$). From a practical perspective, it would be challenging to precisely determine the limit between primary and secondary drying; therefore, this study investigates the effect of radiation initiation point on drying rate and quality attributes. The radiation initiation time of the IRAFD-5.0 kW/m^2 at 10% WR was 125±4 min. Therefore, a sharp decline in the moisture decline curve was observed after this period. The sample temperature of IRAFD-5.0 kW/m^2 at 10% WR increased from –26.4℃ to 34.9℃, which is similar to the temperature profiles of continuous IRAFD. The vacuum energy and radiant energy was 258±11 kJ and 734±11 kJ, respectively (Table 1). IR radiation was started at 125±4 min when the sample weight was reduced by 10%. After the primary drying of the FD process, heat must be added to the sample as more energy is required to eliminate the water, which is more strongly bound during the secondary drying process (Nireesha et al., 2013).

In the IRAFD-5.0 kW/m^2 at 20% WR showed the total drying time 1,168±33 min and 1.55±0.04 g/h of drying rate which reduced the time required for drying by 59% compared to FD with the combined effect of vacuum energy of 409±24 kJ and radiant energy of 583±24 kJ ($p<0.05$). The final temperature was indicated 35.2℃. In this test, the IR radiation was initiated at 390±3 min when the sample weight reduction (WR) reached 20%. Once the IR initiation time is delayed until the controlled WR, more drying time is required.

In the IRAFD-5.0 kW/m^2 at 30% WR, the temperature rose from –28.2℃ to 35.3℃. It required a total drying time of 1,331±52 min and a drying rate of 1.42±0.07 g/h. It saved the total drying time by 53% compared to FD ($p<0.05$). The IR radiation was initiated at 503±8 min when the sample weight was diminished by 30%. IRAFD-5.0 kW at 30% WR reduced the radiant energy compared to that of continuous IRAFD-5.0 kW/m^2 (905,428±5,364 J) ($p<0.05$). This is attributed to the delayed IR initial time until a 30% WR. The appropriate IR initiation time will be discussed later concerning the nutritional and quality aspects (amino acid content and texture). The radiant energy of IRAFD-5.0 kW/m^2 at 30% WR was reduced to 514,460±31,078 J as compared to 905,428±5,364 J of the Continuous IRAFD-5.0 kW/m^2. Application of IR radiation in FD could appreciably decrease drying time and energy consumption (Lin et al., 2005). The IR energy penetrates into product and expands through the material for create molecular vibrations, providing temperature increase with good energy efficiency compared to other types of heat sources (Chakraborty et al., 2011). In this study, all the tested IRAFD experiments reduced the total drying times when compared with FD. This indicates that energy consumption could be reduced by the IRAFD drying system.

Drying kinetics

The calculated coefficients of the tested drying kinetic models (exponential, page, and simplified diffusion model) are summarized in Table 2. Fig. 3 compares the MR versus time between the experimental value and the model fit. All the IRAFD treatments accelerated the drying rate with a higher k value than that of FD. The highest k value of the exponential

Table 2. Coefficient and statistical of estimated model fitting of FD and different IRAFD trials for dried *Protaetia brevitarsis* larva

Model	Method	k (min^{-1})	D_{eff} ×10^{-10} (m^2/s)	N	R^2
Exponential model	FD	0.0008			0.9555
$MR = \exp(-k \cdot t)$	Continuous IRAFD-5.0 kW/m^2	0.0262			0.9635
	IRAFD-5.0 kW/m^2 at 10% WR	0.0040			0.9101
	IRAFD-5.0 kW/m^2 at 20% WR	0.0019			0.8692
	IRAFD-5.0 kW/m^2 at 30% WR	0.0016			0.8628
Page model	FD	0.000042		1.4140	0.9914
$MR = \exp(-k \cdot t^N)$	Continuous IRAFD-5.0 kW/m^2	0.007032		1.3581	0.9759
	IRAFD-5.0 kW/m^2 at 10% WR	0.000049		1.7837	0.9824
	IRAFD-5.0 kW/m^2 at 20% WR	0.00000012		2.2262	0.9902
	IRAFD-5.0 kW/m^2 at 30% WR	0.00000087		2.1513	0.9847
The simplified diffusion model	FD		1.00		0.8402
$MR = (8/\pi^2)\exp[(-\pi^2/L^2) \cdot D \cdot t]$	Continuous IRAFD-5.0 kW/m^2		18.87		0.6964
	IRAFD-5.0 kW/m^2 at 10% WR		5.13		0.7667
	IRAFD-5.0 kW/m^2 at 20% WR		2.90		0.7971
	IRAFD-5.0 kW/m^2 at 30% WR		2.41		0.8114

FD, freeze-drying; IRAFD, infrared assisted freeze-drying; WR, weight reduction.

model was found to be 0.0262 in the continuous IRAFD-5.0 kW/m^2. In the experimental model, the lowest drying constant (k, min^{-1}) of 0.0008 was found in the FD, which indicated the slowest drying rate. It is expected that an increased k value of the exponential model during drying methods took less drying time with highest drying rate (Khampakool et al., 2019; Lin et al., 2005). The magnitude of the k value corresponded to those of radiant energy (Table 1). The saving in the total drying time of food with increasing energy intensity might be due to an elevation in vapor pressure inside of product with raised temperature, resulting in more rapid moisture migration to the product surface (Afolabi et al., 2015). The coefficient of determination (r^2) of FD and Continuous IRAFD-5.0 kW/m^2 showed a good fit of 0.9555 and 0.9635 in the exponential model, respectively. However, r^2 values showed decreasing trends once the initiation time of IR is delayed at IRAFD-5.0 kW/m^2 at 10% WR, IRAFD-5.0 kW/m^2 at 20% WR, and IRAFD-5.0 kW/m^2 at 30% WR. In the IRAFD trials, the slope of the MR curve showed a sharp decline once IR radiation was initiated. The exponential model could not fit this sudden decline without a shape factor.

The page model adopts both the drying constant (k, min^{-1}) and the shape factor (N) to better describe the non-linear drying curve. The Page model has the strong advantage of explaining both downward concave drying curves (N>1) and upward concave curves (N<1) (Khampakool et al., 2019; Park et al., 2013). In this study, FD showed k and N values of 0.000042 min^{-1} and 1.4140, respectively. Continuous IRAFD-5.0 kW/m^2 showed the maximum value of k as 0.007032 m^{-1} and resulted in N value of 1.3581. Once IR radiation time was delayed at IRAFD-5.0 kW/m^2 at 20% WR and 30% WR, N value significantly increased up to 2.2262 and 2.1513 for a strong downward concave curve (Khampakool et al., 2019). A strong downward concave originates in the desorption of moisture with intense IR radiation. This raised N value could better explain the sharp decline in the drying curve with IR initiation. The r^2 values of the Page model ranged from 0.9759 to 0.9914, which were the highest values among the tested models. The Page model presented the least gap between the experimental values

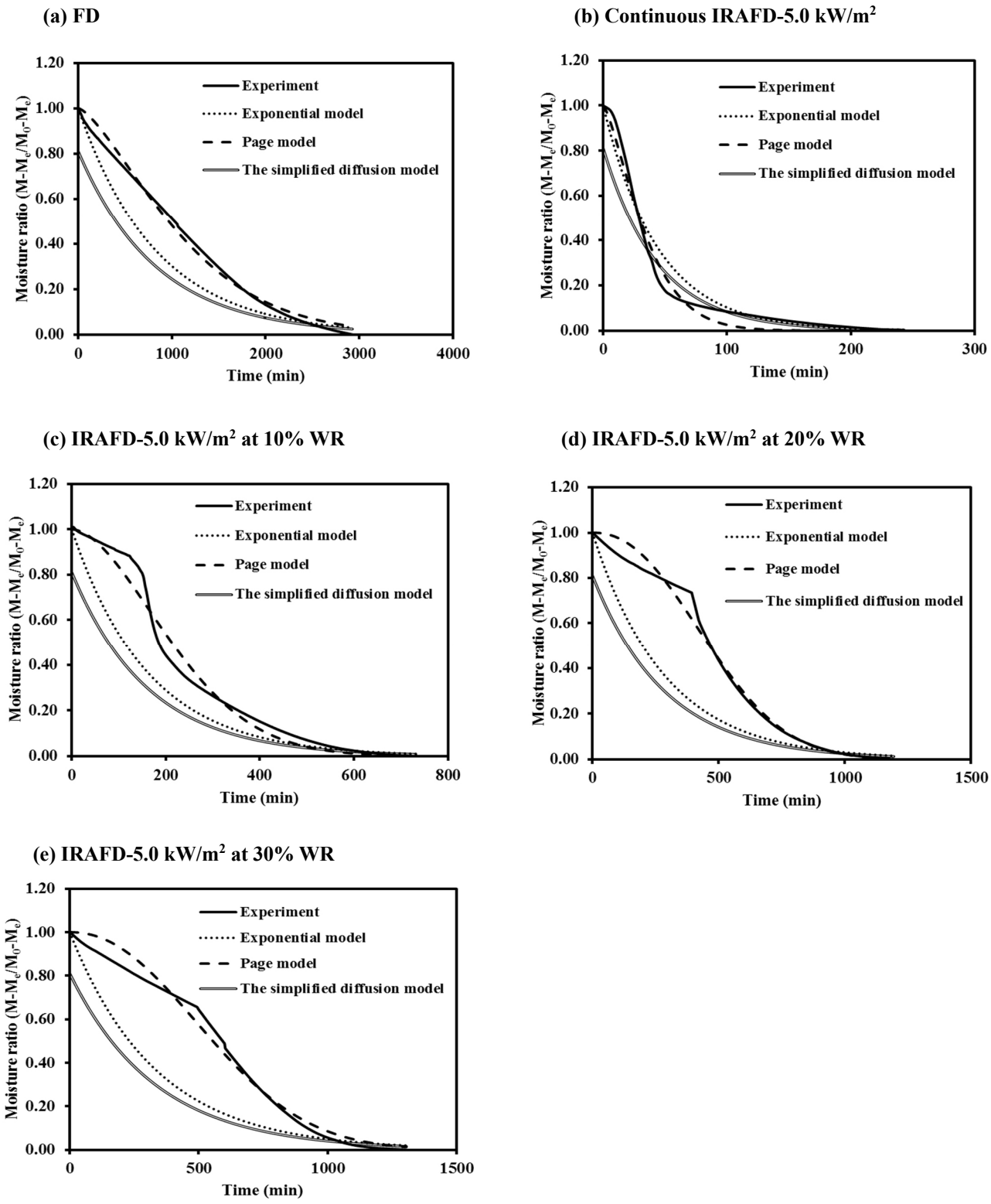

Fig. 3. Comparison of drying curves for *Protaetia brevitarsis* larva between experiment and estimated model fittings. FD, freeze-drying; IRAFD, infrared assisted freeze-drying; WR, weight reduction.

and model fitting (Fig. 3). Previous researchers reported that the page model is the most suitable for describing the drying behavior of fruits and vegetables (Khampakool et al., 2019; Lopez-Quiroga et al., 2019). Ikonić et al. (2012) also found that

the Page model showed good fitting to characterize the drying of meat. In this study, the Page model could be applied to describe the drying behavior of dried insects as well.

In the diffusion model, FD showed the lowest D_{eff} of 1.00×10^{-10} m^2/s. Continuous IRAFD-5.0 kW/m^2 increased the D_{eff} to 18.87×10^{-10} m^2/s. NIR radiation increases thermal energy, which accelerates the vibration of water molecules of insects and creates high moisture diffusivity (Shi et al., 2008). Salehi and Kashaninejad (2018) reported that the D_{eff} values increased with enhanced infrared radiation intensity and time due to the rapid moisture movement at elevated temperatures. The values of D_{eff} are comparable with previous studies data of 4.39 to 9.96×10^{-10} m^2/s for chicken muscle (Ismail, 2017), 6.55×10^{-10} m^2/s to 1.23×10^{-9} m^2/s for fresh tilapia fillets (Guan et al., 2013), 0.85 to 1.75×10^{-10} m^2/s for hull-less seed pumpkin (Sacilik, 2007), 2.92×10^{-10}, and 1.58×10^{-9} m^2/s for lemon slices (Salehi and Kashaninejad, 2018), and 8.039 to 20.618×10^{-10} m^2/s for mushroom (Darvishi et al., 2013). These values are in good agreement with the estimated D_{eff} values for dried insects. In our study, the r^2 of the diffusion model was quite low, ranging from 0.6964 to 0.8402. It showed a relatively large gap between the experimental and estimated model fittings (Fig. 3). As described above, the Page model could best explain the IRAFD drying kinetics with shape factor.

Electrical energy consumption

Table 3 shows the electrical energy usage of the FD and tested IRAFD treatments. The FD process has four main operations: freezing, vacuum, sublimation, and condensing (Ratti, 2001). The highest total electrical energy usage of 113.75×10^3 kJ was found in FD since it took most of the drying time of 2,833 min and the shortest drying rate of 0.65 g/h. Condenser spent more electrical energy (70.26×10^3 kJ) than a vacuum pump (43.49×10^3 kJ). This study showed that all tested IRAFD conditions significantly reduced total electrical energy in comparison to FD ($p<0.05$). The continuous IRAFD-5.0 kW/m^2 consumed the lowest total electrical power of 9.67×10^3 kJ as it took the most rapid drying rate of 7.17 g/h. In the IRAFD, the energy consumption of the IR lamp was minor as compared to those of the vacuum pump and condenser (Khampakool et al., 2019). For example, the energy consumption of the IR lamp was 5.14 kJ, whereas the vacuum pump and condenser used significantly higher energies of 3.78×10^3 kJ and 5.88×10^3 kJ, respectively. IR heating has proven to be an efficient heat transfer to food products by saving processing time and energy costs (Pan et al., 2008), high energy efficacy, rapid heating, uniform heating, simple equipment, and minimized quality loss (Aghajanzadeh et al., 2016; Rastogi, 2012). When the IR energy penetrates into the dried product, the radiation works through the food geometry and induces the material to create molecular movement, providing temperature increase (Chakraborty et al., 2011).

Table 3. Electrical energy consumption of FD and different IRAFD trials for dried *Protaetia brevitarsis* larva

Methods	Vacuum pump ($\times10^3$ kJ)	Condenser ($\times10^3$ kJ)	IR lamp (kJ)	Total ($\times10^3$ kJ)
FD	43.5±1.4^a	70.3±2.2^a	-	113.8±3.5^a
Continuous IRAFD-5.0 kW/m^2	3.8±0.1^e	5.9±0.2^e	5.1±0.2^a	9.7±0.6^e
IRAFD-5.0 kW/m^2 at 10% WR	10.9±0.4^d	18.8±0.8^d	1.7±0.1^b	29.7±1.2^d
IRAFD-5.0 kW/m^2 at 20% WR	16.9±0.5^c	27.1±0.8^c	1.2±0.1^c	44.1±1.2^c
IRAFD-5.0 kW/m^2 at 30% WR	19.3±0.8^b	30.9±1.2^b	1.3±0.1^c	50.2±2.0^b

$^{a-e}$ Means (±SD) with a different letter in the same column are significantly different at $p<0.05$.
FD, freeze-drying; IRAFD, infrared assisted freeze-drying; WR, weight reduction.

Texture analysis, external size, and external appearance

Table 4 summarized the texture analyses (hardness and chewiness) and external size of dried insects with hot air drying (AD), FD, and different IRAFD trials. Hardness and chewiness ranged from 2.68 to 8.26 N and 1.13 to 4.71 N, respectively. All the IRAFD trials showed lower hardness and chewiness than AD and FD ($p<0.05$). However, no significant differences were found among the tested IRAFD trials. Insect texture would be modified by a processing method (Mishyna et al., 2020). AD had the highest hardness and chewiness of 8.26 and 4.71 N, respectively. Convective hot-air dryers are popularly used in the various agricultural product industries. However, hot-air drying might result in physicochemical quality changes and protein denaturation of animal products as the temperature is the most influential factor (FAO, 1995; Mewa et al., 2018). As shown in Fig. 4, AD insect presented significant shrinkage and the least external size of 180 mm^2 as compared to IRAFD trials. The hot air temperature of AD at 70℃ would induce protein denaturation and shrinkage, with the highest values of hardness and chewiness.

Although FD samples showed no significant difference in hardness and chewiness to those of AD ($p>0.05$), FD insects

Table 4. Effect of FD and different IRAFD trials on texture (hardness, chewiness) and external size of dried *Protaetia brevitarsis* larva

Methods	Hardness (N)	Chewiness	External size (mm^2)
AD	8.26±1.71[a]	4.71±1.52[a]	180±4[e]
FD	7.26±1.22[a]	4.59±1.08[a]	262±13[d]
Continuous IRAFD-5.0 W/km^2	5.01±0.90[b]	2.02±0.18[b]	497±19[a]
IRAFD-5.0 W/km^2 at 10% WR	3.47±0.40[b]	1.53±0.39[b]	470±13[b]
IRAFD-5.0 W/km^2 at 20% WR	2.68±0.34[b]	1.13±0.18[b]	465±15[b]
IRAFD-5.0 W/km^2 at 30% WR	3.21±0.68[b]	1.35±0.31[b]	347±10[c]

[a–e] Means (±SD) with a different letter in the same column are significantly different at $p<0.05$.
AD, hot air drying; FD, freeze-drying; IRAFD, infrared assisted freeze-drying; WR, weight reduction.

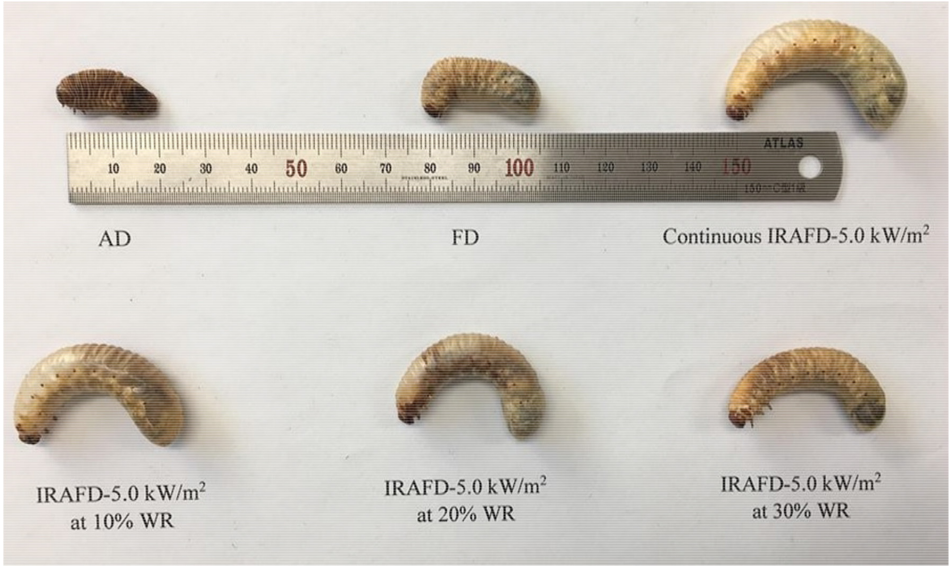

Fig. 4. External appearance of dried *Protaetia brevitarsis* larva during AD, FD, and different IRAFD trials. AD, hot air drying; FD, freeze-drying; IRAFD, infrared assisted freeze-drying; WR, weight reduction.

showed no significant shrinkage as compared to initial size of 270±8 mm^2. In this study, all the IRAFD trials decreased the hardness and chewiness of dried insects as compared to AD and FD. This could be attributed to the volume expansion of IRAFD treated insects, as shown in Fig. 4. Although this study did not focus on the anatomy of insect larvae, radiative energy under vacuum would induce the expansion of space between the external membrane and body of larvae. Continuous IRAFD samples showed the highest volume expansion and external size of 497 mm^2. Consumer expectations might have a significant effect on the textural qualities of unfamiliar foods (Mishyna et al., 2020). For example, people who expected to experience the crispy texture of mealworms evaluated this texture positively. Hence, those who preferred a meat-like texture negatively evaluated mealworms (Mishyna et al., 2020).

Protein and amino acid contents

The protein content is shown in Fig. 5. The results show that IRAFD-5.0 kW/m^2 at 30% WR had the highest protein content of 58.5±3.5 g/100 g. When a protein solution is slowly heated over critical temperature, it induces a sharp transition from the native state to the denatured state with irreversible protein denaturation, loss in biological activity, and solubility (Abdul-Fattah et al., 2007). *P. brevitarsis* larva showed that a high amount of protein might be used as a valuable alternative dietary source.

Valine has the highest concentrations ranging from 3.12 g to 3.75 g/100 g among the essential amino acids (Fig. 6A). Among the non-essential amino acids (Fig. 6B), the amino acid of *P. brevitarsis* larva was found to be high in glutamic acid (6.30–7.29 g/100 g) and proline (3.84–5.54 g/100 g). Of the non-essential amino acids, glutamic acid, in agreement with other scientific reports, was found to be dominant (Chung et al., 2013; Ghosh et al., 2017). For example, Ghosh et al. (2017) found that the highest glutamic acid content of *P. brevitarsis* larva (5.54 g/100 g), *T. molitor* (5.78 g/100 g), and *G. bimaculatus* (6.39 g/100 g). In contrast, cysteine has the lowest concentrations ranging from 0.71g to 0.83 g/100 g. Similarly,

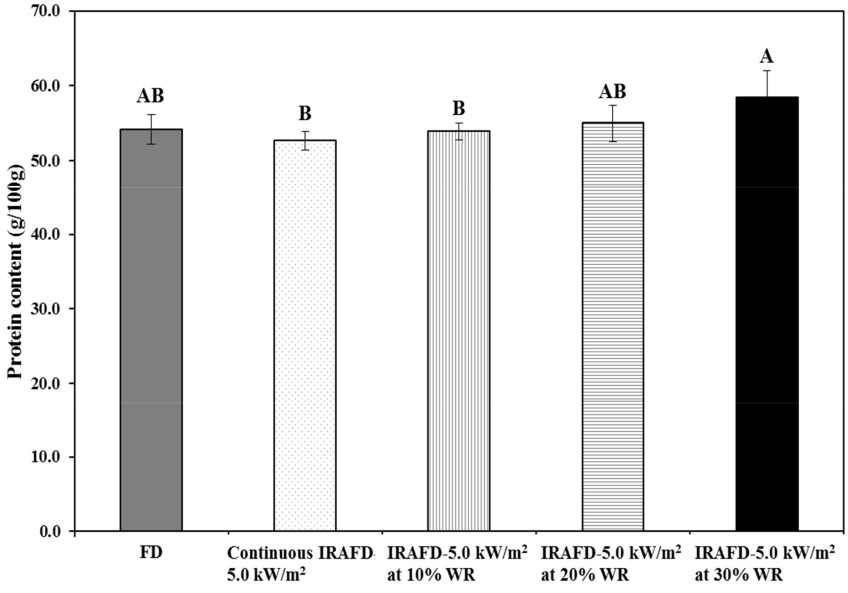

Fig. 5. Protein content (g/100 g) of dried *Protaetia brevitarsis* larva during AD, FD, and different IRAFD trials. A,B Means (±SD) with a different letter are significantly different at $p<0.05$. AD, hot air drying; FD, freeze-drying; IRAFD, infrared assisted freeze-drying; WR, weight reduction.

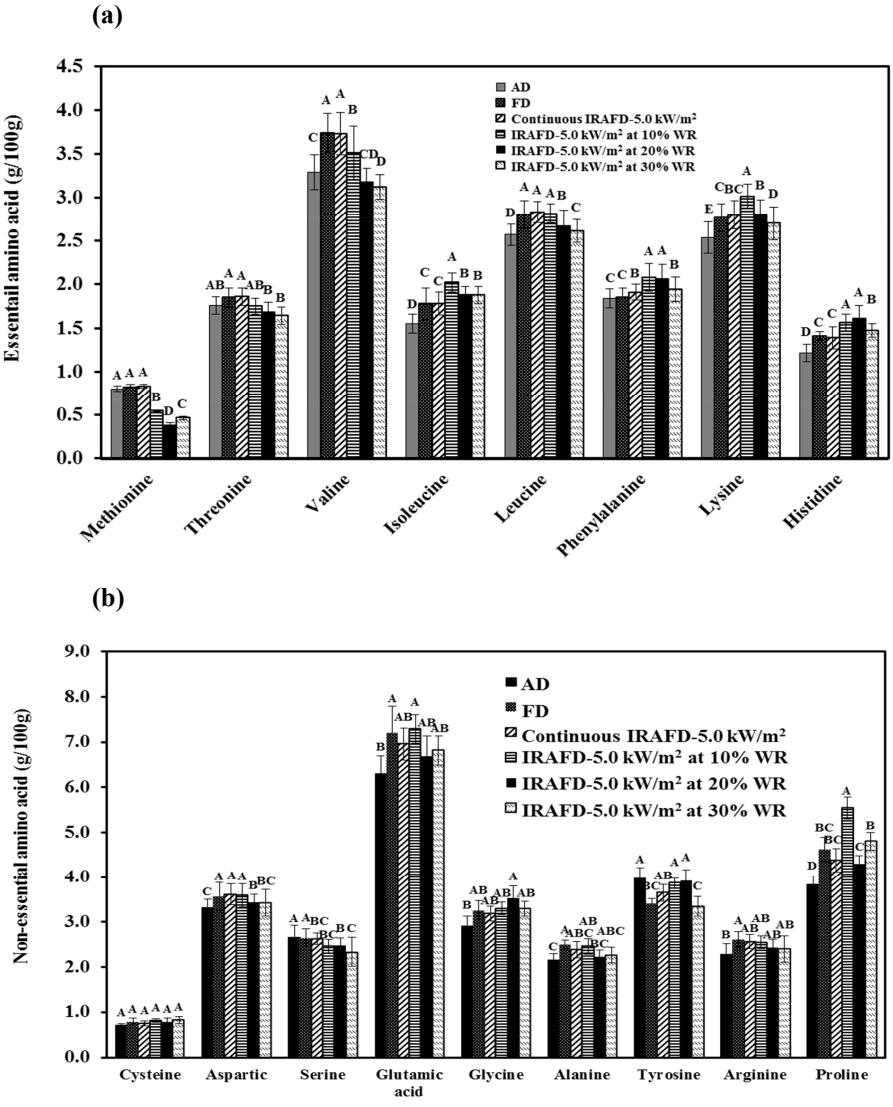

Fig. 6. Essential (a) and non-essential amino acid (b) contents of dried *Protaetia brevitarsis* larva during AD, FD, and different IRAFD trials. $^{A–D}$ Means (±SD) with a different letter are significantly different at $p<0.05$. AD, hot air drying; FD, freeze-drying; IRAFD, infrared assisted freeze-drying; WR, weight reduction.

a study by Köhler et al. (2019) showed that cysteine has the lowest values in the Bombay locust (0.19 g/100 g), scarab beetle (0.35 g/100 g), house cricket (0.49 g/100 g), and mulberry silkworm (0.61 g/100 g). All IRAFD trials had glutamic acid and proline levels higher than those of AD. Proline is regarded as an energy supplment for protein synthesis and has a major role in invertebrates (Osanai and Yonezawa, 1986). Insects could consume proline in their diet and utilize it as an energy source to fly and other high-energy activities (Carter et al., 2006; Darvishzadeh et al., 2015). For humans, proline is one of the principal amino acids that the body uses to build collagen (Chung et al., 2013). Glutamic acid is the major neurotransmitter in the central nervous system and is associated with learning and memory (Dutta et al., 2013).

Conclusion

The IRAFD system exhibited good potential for the production of value-added shelf-stable insect foods. The IRAFD

system was found to significantly ($p<0.05$) reduce the drying rate when compared to FD alone. For example, continuous IRAFD-5.0 kW/m^2 saved the time required for drying by 90% compared with conventional FD. The thin layer drying kinetics of dried insects was studied during FD and different IRAFD trials. The results showed that the Page model explained the best the drying kinetics of dried insects. Values for the effective moisture diffusivity (D_{eff}) of dried insects were obtained in the range of 1–18.87×10^{-10} m^2/s. Concerning the textural quality, IRAFD showed lower hardness, chewiness, and higher protein content levels than AD and FD. In IRAFD-5.0 kW/m^2 at 10% WR, glutamic acid (6.30–7.29 g/100 g) and proline (3.84–5.54 g/100 g) were found in high concentrations. The external product appearance after IRAFD showed more air pockets and volume expansion compared to the AD-derived product, which might result in a good consumer appeal for dried snack products.

Conflicts of Interest

The authors declare no potential conflicts of interest.

Acknowledgements

This study was supported by the Advanced Research Project funded by the SeoulTech (Seoul National University of Science and Technology).

Author Contributions

Conceptualization: Khampakool A, Park SH. Formal analysis: Khampakool A. Methodology: Khampakool A, Soisungwan S. Validation: You SG, Park SH. Investigation: Khampakool A, Park SH. Writing-origanl draft: Khampakool A. Writing-review & editing: Khampakool A, Soisungwan S, You SG, Park SH.

Ethics Approval

This article does not require IRB/IACUC approval because there are no human and animal participants.

References

Abdul-Fattah AM, Kalonia DS, Pikal MJ. 2007. The challenge of drying method selection for protein pharmaceuticals: Product quality implications. J Pharmaceut Sci 96:1886-1916.

Afolabi TJ, Tunde-Akintunde TY, Adeyanju JA. 2015. Mathematical modeling of drying kinetics of untreated and pretreated cocoyam slices. J Food Sci Technol 52:2731-2740.

Aghajanzadeh S, Kashaninejad M, Ziaiifar AM. 2016. Effect of infrared heating on degradation kinetics of key lime juice physicochemical properties. Innov Food Sci Emerg Technol 38:139-148.

Alves AV, Sanjinez-Argandoña EJ, Linzmeier AM, Cardoso CAL, Macedo MLR. 2016. Food value of mealworm grown on *Acrocomia aculeata* pulp flour. PLOS ONE 11:e0151275.

AOAC. 2016. Official methods of analysis of AOAC International. AOAC International, Gaithersburg, MD, USA.

Baeghbali V, Ngadi M, Niakousari M. 2020. Effects of ultrasound and infrared assisted conductive hydro-drying, freeze-drying and oven drying on physicochemical properties of okra slices. Innov Food Sci Emerg Technol 63:1-8.

Baiano A. 2020. Edible insects: An overview on nutritional characteristics, safety, farming, production technologies, regulatory framework, and socio-economic and ethical implications. Trends Food Sci Technol 100:35-50.

Carter C, Shafir S, Yehonatan L, Palmer RG, Thornburg R. 2006. A novel role for proline in plant floral nectars. Naturwissenschaften 93:72-79.

Chakraborty R, Bera M, Mukhopadhyay P, Bhattacharya P. 2011. Prediction of optimal conditions of infrared assisted freeze-drying of aloe vera (*Aloe barbadensis*) using response surface methodology. Sep Purif Technol 80:375-384.

Chang SKC. 2010. Protein analysis. In Food analysis. Springer, New York, NY, USA. pp 133-146.

Chung MY, Hwang JS, Goo TW, Yun EY. 2013. Analysis of general composition and harmful material of *Protaetia brevitarsis*. J Life Sci 23:664-668.

Ciurzyńska A, Lenart A. 2011. Freeze-drying - application in food processing and biotechnology: A review. Polish J Food Nutr Sci 61:165-171.

Darvishi H, Najafi G, Hosainpour A, Khodaei J, Aazdbakht M. 2013. Far-infrared drying characteristics of mushroom slices. Chem Prod Proc Model 8:107-117.

Darvishzadeh A, Hosseininaveh V, Nehzati G, Nozari J. 2015. Effect of proline as a nutrient on hypopharyngeal glands during development of *Apis mellifera* (Hymenoptera: Apidae). Arthropods 4:137-143.

Doymaz I. 2011. Drying of eggplant slices in thin layers at different air temperatures. J Food Proc Pres 35:280-289.

Dutta S, Ray S, Nagarajan K. 2013. Glutamic acid as anticancer agent: An overview. Saudi Pharmaceut J 21:337-343.

FAO. 1995. Development and promotion of value added products. Project Document. Rome: 509 Food and Agriculture Organization of the United Nations, Rome, Italy.

Ghosh S, Lee SM, Jung C, Meyer-Rochow VB. 2017. Nutritional composition of five commercial edible insects in South Korea. J Asia-Pac Entomol 20:686-694.

Guan Z, Wang X, Li M, Jiang X. 2013. Mathematical modeling on hot air drying of thin layer fresh tilapia fillets. Polish J Food Nutr Sci 63:25-33.

Hafezi N, Sheikhdavoodi MJ, Sajadiye SM, Ferdavani MEK. 2014. Evaluation of energy consumption of potato slices drying using vacuum-infrared method. Int J Adv Biolo Biomed Res 2:2651-2658.

Ikonić P, Petrović L, Tasić T, Jokanović M, Savatić S, Ikonić B, Džinić N. 2012. The effect of processing method on drying kinetics of *Petrovská klobása*, an artisan fermented sausage. Chem Ind Chem Eng Q 18:163-169.

Ismail O. 2017. An experimental and modeling investigation on drying of chicken meat in convective dryer. Stud Univ Babes-Bol Chem 62:459-469.

Jeong D, Min N, Kim Y, Kim SR, Kwon O. 2020. The effects of feed materials on the nutrient composition of *Protaetia brevitarsis* larvae. Entomol Res 50:23-27.

Jin J, Yurkow EJ, Adler D, Lee TC. 2018. Improved freeze drying efficiency by ice nucleation proteins with ice morphology modification. Food Res Int 106:90-97.

Kashaninejad M, Mortazavi A, Safekordi A, Tabil LG. 2007. Thin-layer drying characteristics and modeling of pistachio nuts. J Food Eng 78:98-108.

Khampakool A, Soisungwan S, Park SH. 2019. Potential application of infrared assisted freeze drying (IRAFD) for banana snacks: Drying kinetics, energy consumption, and texture. LWT-Food Sci Technol 99:355-363.

Klunder HC, Wolkers-Rooijackers J, Korpela JM, Nout MJR. 2012. Microbiological aspects of processing and storage of edible insects. Food Control 26:628-631.

Köhler R, Kariuki L, Lambert C, Biesalski HK. 2019. Protein, amino acid and mineral composition of some edible insects from Thailand. J Asia-Pac Entomo 22:372-378.

Kröncke N, Böschen V, Woyzichovski J, Demtröder S, Benning R. 2018. Comparison of suitable drying processes for mealworms (*Tenebrio molitor*). Innov Food Sci Emerg Technol 50:20-25.

Lee J, Hwang IH, Kim JH, Kim MA, Hwang JS, Kim YH, Na M. 2017. Quinoxaline-, dopamine-, and amino acid-derived metabolites from the edible insect *Protaetia brevitarsis seulensis*. Arch Pharm Res 40:1064-1070.

Lin YP, Tsen JH, King VAE. 2005. Effects of far-infrared radiation on the freeze-drying of sweet potato. J Food Eng 68:249-255.

Lopez-Quiroga E, Prosapio V, Fryer PJ, Norton IT, Bakalis S. 2020. Model discrimination for drying and rehydration kinetics of freeze-dried tomatoes. J Food Proc Eng 43:e313192.

Melis R, Braca A, Mulas G, Sanna R, Spada S, Serra G, Leonarda Fadda M, Roggio T, Uzzau S, Anedda R. 2018. Effect of freezing and drying processes on the molecular traits of edible yellow mealworm. Innov Food Sci Emerg 48:138-149.

Mewa EA, Okoth MW, Kunyanga CN, Rugiri MN. 2018. Effect of drying air temperature and slice thickness on the physical and microbiological quality of dried beef. LWT-Food Sci Technol 92:484-489.

Mishyna M, Chen J, Benjamin O. 2020. Sensory attributes of edible insects and insect-based foods-Future outlooks for enhancing consumer appeal. Trends Food Sci Technol 95:141-148.

Nireesha GR, Divya L, Sowmya C, Venkateshan N, Niranjan Babu M, Lavakumar V. 2013. Lyophilization/freeze drying: An review. Int J Novel Trend Pharm Sci 3:87-98.

Osanai M, Yonezawa Y. 1986. Changes in amino acid pools in the silkworm, *Bombyx mori* during embryonic life: Alanine accumulation and its conversion to proline during diapause. Insect Biochem 16:373-379.

Page GE. 1949. Factors influencing the maximum rates of air drying shelled corn in thin layers. M.S. thesis, Purdue Univ., West Lafayette, IN, USA.

Pan Z, Shih C, McHugh TH, Hirschberg E. 2008. Study of banana dehydration using sequential infrared radiation heating and freeze-drying. LWT-Food Sci Technol 41:1944-1951.

Park SH, Balasubramaniam VM, Sastry SK. 2014. Quality of shelf-stable low-acid vegetables processed using pressure-ohmic-thermal sterilization. LWT-Food Sci Technol 57:243-252.

Park SH, Jo YJ. 2019. Static hydrothermal processing and fractionation for production of a collagen peptide with anti-oxidative and anti-aging properties. Process Biochem 83:176-182.

Park SH, Balasubramaniam VM, Sastry SK, Lee J. 2013. Pressure-ohmic-thermal sterilization: A feasible approach for the inactivation of *Bacillus amyloliquefaciens* and *Geobacillus stearothermophilus* spores. Innov Food Sci Emerg Technol 19:115-123.

Rastogi NK. 2012. Recent trends and developments in infrared heating in food processing. Crit Rev Food Sci Nutr 52:737-760.

Ratti C. 2001. Hot air and freeze-drying of high-value foods: A review. J Food Eng 49:311-319.

Sacilik K. 2007. Effect of drying methods on thin-layer drying characteristics of hull-less seed pumpkin (*Cucurbita pepo* L.). J Food Eng 79:23-30.

Shi J, Pan Z, McHugh TH, Wood D, Hirschberg E, Olson D. 2008. Drying and quality characteristics of fresh and sugar-

infused blueberries dried with infrared radiation heating. LWT-Food Sci Technol 41:1962-1972.

Simal S, Femenia A, Garau MC, Rosselló C. 2005. Use of exponential, Page's and diffusional models to simulate the drying kinetics of kiwi fruit. J Food Eng 66:323-328.

Vandeweyer D, Lenaerts S, Callens A, Van Campenhout L. 2017. Effect of blanching followed by refrigerated storage or industrial microwave drying on the microbial load of yellow mealworm larvae (*Tenebrio molitor*). Food Control 71:311-314.

Wang Q, Li S, Han X, Ni Y, Zhao D, Hao J. 2019. Quality evaluation and drying kinetics of shitake mushrooms dried by hot air, infrared and intermittent microwave-assisted drying methods. LWT-Food Sci Technol 107:236-242.

Yeo H, Youn K, Kim M, Yun EY, Hwang JS, Jeong WS, Jun M. 2013. Fatty acid composition and volatile constituents of *Protaetia brevitarsis* larvae. Prev Nutri Food Sci 18:150-156.

Zdunkowski W, Bott A. 2004. Thermodynamics of the atmosphere. Cambridge University Press, Cambridge, UK. p 245.

Zielińska E, Baraniak B, Karaś M, Rybczyńska K, Jakubczyk A. 2015. Selected species of edible insects as a source of nutrient composition. Food Res Int 77:460-466.